Platinum nanoparticle-functionalized tin dioxide nanowires via radiolysis and their sensing capability

Sun-Woo Choi and Sang Sub Kim[a)]
School of Materials Science and Engineering, Inha University, Incheon 402-751, Republic of Korea

(Received 23 September 2011; accepted 19 April 2012)

Platinum (Pt) nanoparticles were synthesized on tin dioxide (SnO_2) nanowires by applying γ-ray radiolysis. The growth behavior of Pt nanoparticles was systematically investigated as a function of precursor concentration, illumination intensity and exposure time of the γ-rays. We found that these processing parameters greatly influenced the growth behavior of Pt nanoparticles in terms of size and formation density. Vapor-phase-grown SnO_2 nanowires were uniformly covered with Pt nanoparticles by the radiolysis process. The Pt nanoparticle-functionalized SnO_2 nanowires were tested as sensors for detecting reductive gases including carbon monoxide, toluene, and benzene. The results indicate that the γ-ray radiolysis is an efficient way of functionalizing the surface of oxide nanowires with catalytic Pt nanoparticles.

I. INTRODUCTION

In recent years, various shapes of nanomaterials have received increased attention due to their unique physical and chemical properties, which are significantly different from their bulk or thin film counterparts. In particular, noble metal nanoparticles are attracting considerable interests from researchers owing to their various potential surface-related catalytic applications.

As of date, for synthesizing metal nanoparticles, various methods such as photochemistry,[1] reverse micelles,[2] arc discharge,[3] radiolysis[4] and sonochemistry[5] have been attempted. According to the literature survey,[6–8] some research groups have succeeded in synthesizing metal nanoparticles by the γ-ray radiolysis process. Henglein reported the synthesis of ultrafine colloidal Au nanoparticles in aqueous solutions under a γ-ray illumination of 1.8×10^6 rad/h for 4 min.[6] Seino et al.[8] successfully prepared Au/γ-Fe_2O_3 composite nanoparticles via the radiolysis process.

Metallic catalysts are known to functionalize the surface of nanomaterials. For instance, noble metals anchored on semiconducting oxides facilitate the dissociation of oxygen molecules into oxygen species, including atomic oxygen, thereby enhancing the oxygen sensitivity.[9,10] Accordingly, some research groups have attempted to functionalize the surface of nanowires with nanosized noble metals using various methods.[11–13]

Platinum (Pt) nanoparticles were tested in the design of chemical sensors,[14–16] on the premise that they can promote electron transfer and thus enhance mass transport characteristics.[14,17–20] For instance, Ikariyama et al.[17] proved Pt nanoparticles as an excellent matrix for microenzyme sensors. Wang et al.[18] reported ultrafine Pt particles-modified carbon fibers for detecting hydrazine (N_2H_4). In addition, Birkin et al.[20] demonstrated that Pt nanoparticles could be used in combination with single-wall carbon nanotubes for constructing electrochemical sensors with a remarkably improved sensitivity to H_2O_2.

Although the addition of noble metals to SnO_2 nanowires is known to enhance gas sensitivity of SnO_2, to the best of our knowledge, no work has been reported on Pt-functionalization via the γ-rays radiolysis on SnO_2 nanowires. In the present work, we have applied γ-ray radiolysis to synthesize Pt nanoparticles on SnO_2 nanowires. The growth behavior of Pt nanoparticles was systematically investigated as a function of the precursor concentration, illumination intensity, and exposure time of the γ-rays. Sensing capabilities of the Pt-functionalized SnO_2 nanowires were investigated for carbon monoxide (CO), toluene and benzene.

II. EXPERIMENTAL PROCEDURE

For the γ-ray radiolysis, the precursor solutions were prepared as follows. Various contents ranging from 0.25 to 2.0 mM of hydrogen hexachloroplatinate (IV) hydrate ($H_2PtCl_6 \cdot nH_2O$, $n = 5.8$, Kojima Chemicals Co., Sayama, Japan) were dissolved in a mixed solvent of deionized water (94 vol%) and 2-propanol (6 vol%). The prepared solutions were stirred for 24 h, and subsequently illuminated with ^{60}Co γ-rays under an air ambient condition at room temperature. This was done at the Korea Atomic Energy Research Institute (KAERI).

For investigating the growth behavior of Pt nanoparticles using radiolysis in a systematic fashion, the

[a)]Address all correspondence to this author.
e-mail: sangsub@inha.ac.kr
DOI: 10.1557/jmr.2012.148

 © Materials Research Society 2012

https://doi.org/10.1557/jmr.2012.148 Published online by Cambridge University Press

γ-ray illumination conditions, including the precursor concentration and the intensity and exposure time of the γ-rays were varied while the other conditions were held constant. Si wafers were used to support the Pt nanoparticles synthesized in the solutions. For the functionalization of the surface of SnO_2 nanowires with the Pt nanoparticles, SnO_2 nanowires were immersed into solutions of various precursor concentrations. The γ–ray conditions used were as follows; Exposure time: 1–4 h at 10 kGy/h and 1.0 mM $H_2PtCl_6{\cdot}nH_2O$; Illumination intensity: 2–15 kGy/h at 1.0 mM $H_2PtCl_6{\cdot}nH_2O$ for 2 h. After the γ-ray illumination, the samples were taken out of the solution container and heat-treated at 500 °C for 1 h in an air atmosphere to remove solvents or precursors that may remain on the surface of the samples.[21]

SnO_2 nanowires were grown by a typical vapor–liquid–solid (VLS) process in a horizontal tube furnace. Au-coated Si wafers were placed in the tube furnace along with an alumina boat containing Sn powders of less than 150 μm in average diameter (Sigma-Aldrich Co., St. Louis, MO). Thereafter, the growth of SnO_2 nanowires was performed at 900 °C for 0.5 h under 4–6 Torr of flowing O_2 [~10 standard cubic centimeter per minute (sccm)] and N_2 (~300 sccm). The experimental condition used in synthesizing SnO_2 nanowires in this study has been described in detail in our previous reports.[22,23]

For the sensor fabrication, networked SnO_2 nanowires were selectively grown by the VLS growth method on patterned interdigital electrodes (PIEs) made on SiO_2-grown Si (100) substrates using a conventional photolithographic process. The electrodes were trilayers consisting of Au (3 nm)/Pt (100 nm)/Ti (100 nm) that had sequentially been deposited by a sputtering method. The Au top layer served as a catalytic layer for the selective growth. A more detailed procedure for the sensor fabrication is described in our previous publications.[23]

The resistance change of the Pt-functionalized SnO_2 nanowires to CO, toluene and benzene were measured at 300 °C under various gas concentrations using a custom-made gas sensing system. The response (R) was estimated as $R = R_a/R_g$, where R_a is the initial resistance in the absence of target gases and R_g is the resistance measured in the presence of target gases. The microstructure and phase of the synthesized Pt nanoparticles were examined by field-emission scanning electron microscopy (FE-SEM, Hitachi, S-4200, Tokyo, Japan), transmission electron microscopy (TEM, Philips CM-200, Amsterdam, Netherlands) and x-ray diffraction (XRD, Philips X'pert MRD diffractometer, Almelo, Netherlands), respectively. An image analysis system was used to measure the particle size. FE-SEM pictures were input to the system, then more than 200 individual particles were picked up and their diameters were calculated through an image-analysis software. Synthesized Pt particles were often agglomerated. Individual particles could be identified in the image analysis system.

III. RESULTS AND DISCUSSION

In the first place, the growth behavior of Pt nanoparticles has been investigated as a function of radiolysis conditions. Figure 1 shows typical FE-SEM images of Pt nanoparticles synthesized on Si (100) substrates with different precursor concentrations at a γ-ray intensity of 10 kGy/h for 3 h. As is shown, nanoparticles are distributed on the substrates also showing small portions of nanoparticles as agglomerated. The diameter and the formation density, i.e., the number of nanoparticles per unit area are summarized in Fig. 2. Lower concentrations of $H_2PtCl_6{\cdot}nH_2O$ tend to produce Pt nanoparticles of smaller sizes. In contrast, lower concentrations bring about increased formation density.

Figure 3 shows the results for Pt nanoparticles synthesized at various intensities and γ-ray exposure times: (a) various γ-ray intensities for 4 h at 1.0 mM $H_2PtCl_6{\cdot}nH_2O$, (b) various exposure times at 10 kGy/h γ-ray and 0.1 mM $H_2PtCl_6{\cdot}nH_2O$. To avoid repetition, only some of the FE-SEM images are presented as the insets. As clearly shown in Fig. 3, higher intensities lead to smaller Pt nanoparticles. In addition, the Pt nanoparticles gradually increase in size with a prolonged γ-ray exposure time. The formation density shows reverse behavior as regards the size of the nanoparticles.

For understanding the growth behavior of Pt nanoparticles observed in this study, a mechanism of forming metal nanoparticles by γ-ray radiolysis is proposed, as is schematically illustrated in Fig. 4. At the initial stage of illumination, electrons are likely to be generated by water radiolysis.[24,25] The electrons easily reduce the metal ions dissolved in the solutions because they play the role of strong reducing agents. The reduced neutral metal atoms encounter each other by diffusion, consequently forming an embryo because the binding energy between two metal atoms is generally stronger than that of the atom-solvent. A further supply of reduced neutral metal atoms to the embryo produces metal nuclei that are thermodynamically stable. The nuclei grow and then coalesce at the expense of their smaller counterparts, eventually forming metal nanoparticles. On a basis of this radiolysis process, our results can be explained. At higher precursor concentrations, the rate of producing neutral atoms in the precursor solution is higher, suggesting that more atoms diffuse into the nuclei, accordingly generating larger nanoparticles. At a fixed precursor concentration, higher γ-ray intensities yield smaller nanoparticles. The rapid reduction by the high γ-ray intensity leads to a high supersaturation, eventually causing higher nucleation rates and thus smaller particles. A similar result was reported in synthesis of Ag particles using γ-ray radiolysis.[26] In addition, the influence of reduction rate on particle size also follows the general trend often observed in nanoparticle synthesis by chemical reduction methods.[27]

https://doi.org/10.1557/jmr.2012.148 Published online by Cambridge University Press

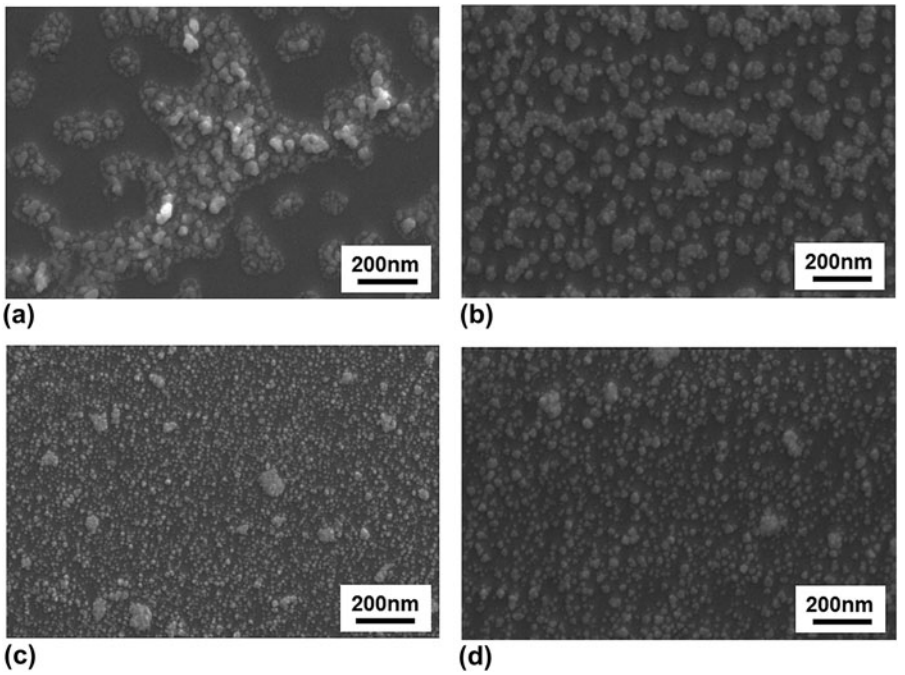


FIG. 1. FE-SEM images of Pt nanoparticles synthesized at a γ-ray intensity of 10 kGy/h for 3 h with different precursor concentrations; (a) 0.25, (b) 0.5, (c) 1.0 and (d) 2.0 mM.

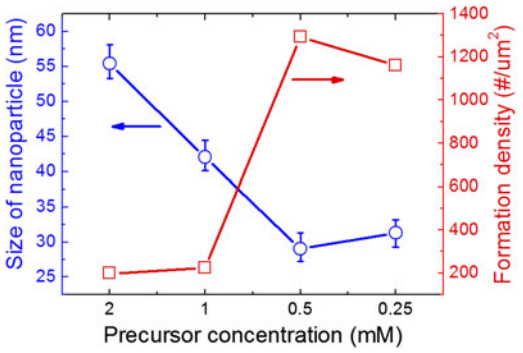


FIG. 2. Plots of the size and the formation density of Pt nanoparticles as a function of precursor concentration.

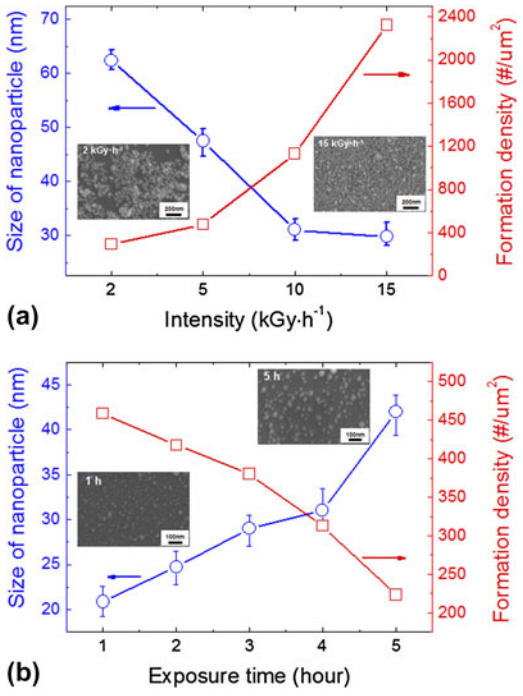


FIG. 3. Plots of the size and the formation density of Pt nanoparticles as a function of (a) γ-ray intensity and (b) γ-ray exposure time. Inset figures are FE-SEM images of some of Pt nanoparticles.

XRD was used to confirm the phase of nanoparticles synthesized in this study. A typical XRD pattern obtained from the sample synthesized at 10 kGy/h for 3 h in a precursor concentration of 1.0 mM is shown in Fig. 5(a). For comparison, an XRD pattern obtained from a Pt film deposited on Si (100) by sputtering is included. There is no difference between the XRD pattern from Pt nanoparticles and that from the film sample, indicating that the nanoparticles synthesized in this study are Pt phase. The Pt nanoparticles were further investigated by TEM and typical results are shown in Fig. 5(b). The inset of Fig. 5(b) is a high-resolution TEM image, which highlights the single crystalline nature of the individual Pt nanoparticles without revealing any significant structural defects such as dislocations or stacking faults. The particle size estimated from the line broadening of the (111) peak of the Pt nanoparticles in Fig. 5(a), based on the Scherrer's equation,[28] was ~15 nm, which is in a good agreement with the size in the TEM observation. These XRD and

https://doi.org/10.1557/jmr.2012.148 Published online by Cambridge University Press

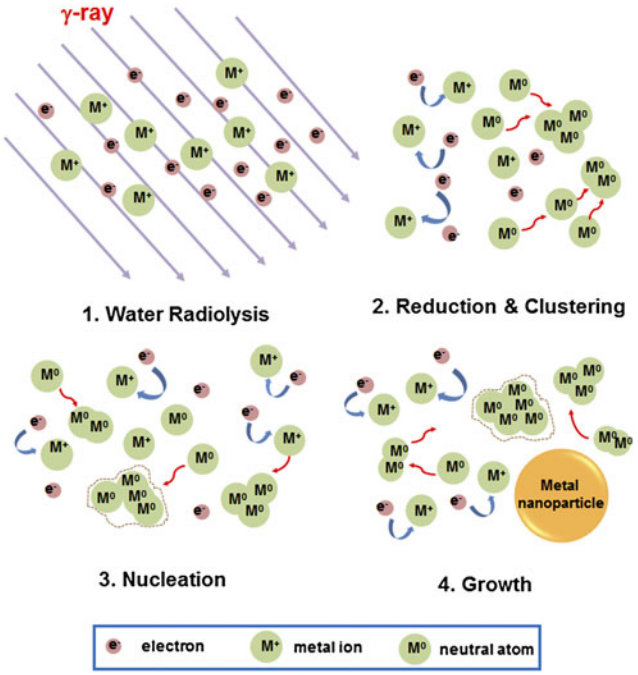


FIG. 4. Schematic pictures illustrating the formation and growth of metallic nanoparticles in the solution by the γ-ray radiolysis.

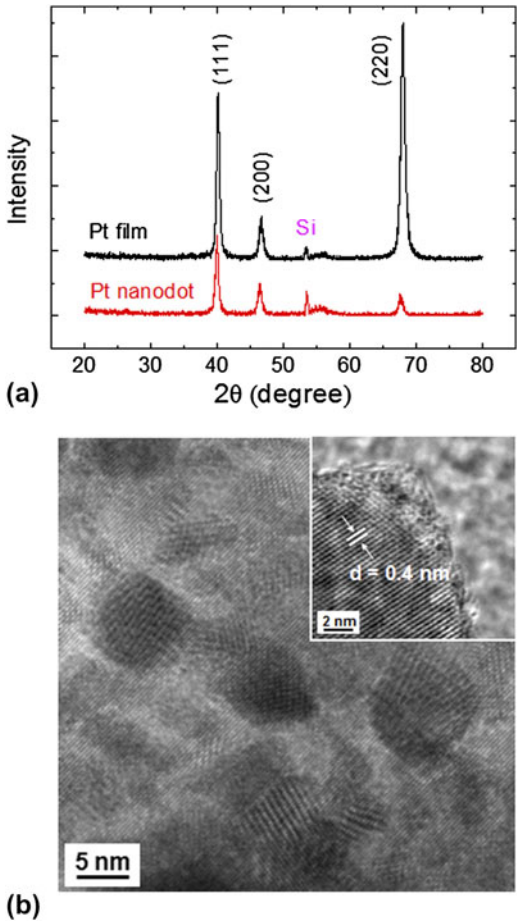


FIG. 5. (a) An x-ray θ-2θ diffraction pattern of Pt nanoparticles. For comparison, an XRD pattern obtained from a Pt thin film is included. (b) A TEM image of the Pt nanoparticles. The inset is a high-resolution TEM image, showing the single-crystalline nature of Pt nanoparticles.

TEM results demonstrate that the Pt nanoparticles synthesized by radiolysis were of high crystalline quality.

Using a typical radiolysis condition used in this study (1.0 mM $H_2PtCl_6 \cdot nH_2O$, 10 kGy/h and 2 h), Pt nanoparticles were synthesized on SnO_2 nanowires. They were grown selectively on the surface of SnO_2 nanowires by heterogeneous nucleation. Figure 6(a) shows the microstructure of Pt nanoparticles-covered SnO_2 nanowires after the radiolysis process. It is evident that nanoparticles are uniformly distributed on the surfaces of every single SnO_2 nanowire. The inset of Fig. 6(a) reveals pristine SnO_2 nanowires. Figure 6(b) shows a TEM image taken from a Pt nanoparticles-covered SnO_2 nanowire before being annealed at 500 °C for 1 h in air, that is, as-synthesized one. It is evident that Pt particles are created on the nanowire surface. Figures 6(c) and 6(d) respectively show TEM images of low and high magnifications, taken from the Pt nanoparticles-covered SnO_2 nanowires after the annealing treatment. The black dots in Fig. 6(c) reveal Pt nanoparticles that appear well anchored on the surfaces of SnO_2 nanowires. No significant difference in light of microstructure between before and after the annealing treatment is observed. Figures 7(a) and 7(b) show XRD patterns taken from the samples of Fig. 6 before and after the annealing treatment, respectively. All of the diffraction peaks are well indexed to the tetragonal rutile structure of SnO_2 and face centered cubic structure of Pt, regardless of the annealing treatment. Based on the TEM and the XRD results, it is reasonable to conclude that as-synthesized Pt nanoparticles by the γ-ray radiolysis are crystalline. Therefore, the major role of the annealing treatment is to remove the residual solvents and precursors.[21] However, a slight improvement in crystallinity of the Pt nanoparticles cannot be excluded during the annealing treatment.

The sensing capabilities of the Pt-functionalized SnO_2 nanowires were investigated at 300 °C in terms of CO, toluene and benzene. The microstructure of the fabricated sensor is shown in Fig. 8. It is evident that between the PIEs, networking of SnO_2 nanowires is created. Pt nanoparticles were synthesized on SnO_2 nanowires by use of the same γ-ray radiolysis condition of Fig. 6. The sensing performances of the sensor are shown in Fig. 9. As shown in Fig. 9(a), when the sensor is exposed to the reductive gases tested in this work, the resistance drops immediately. When the supply of the reductive gases is stopped and air is supplied, the resistance completely recovers to the initial value. Figure 9(b) summarizes the responses as a function

https://doi.org/10.1557/jmr.2012.148 Published online by Cambridge University Press

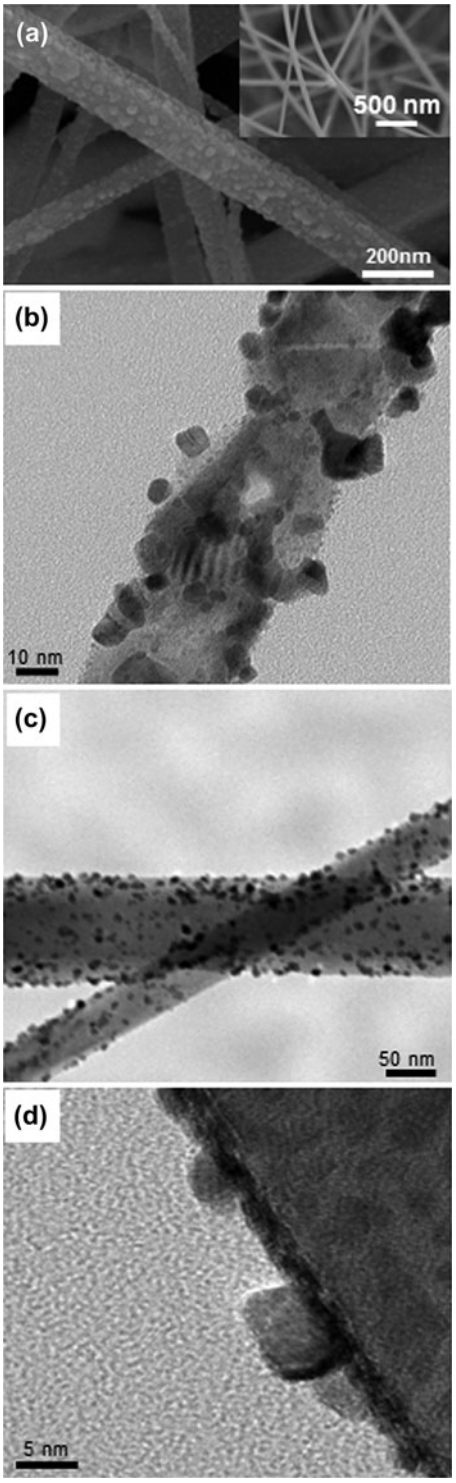


FIG. 6. Microstructures of Pt nanoparticles synthesized by a typical radiolysis condition used in this study (1.0 mM $H_2PtCl_6 \cdot nH_2O$, 10 kGy/h and 2 h). (a) A typical FE-SEM image of Pt nanoparticles decorated on SnO_2 nanowires. The inset figure is an image obtained from pristine SnO_2 nanowires. (b) A TEM image taken from a Pt nanoparticles-covered SnO_2 nanowire before being annealed at 500 °C for 1 h in air. (c) A TEM image of Pt nanoparticles decorated on SnO_2 nanowires. (d) A high-resolution TEM image taken from an individual Pt nanoparticles-decorated SnO_2 nanowire.

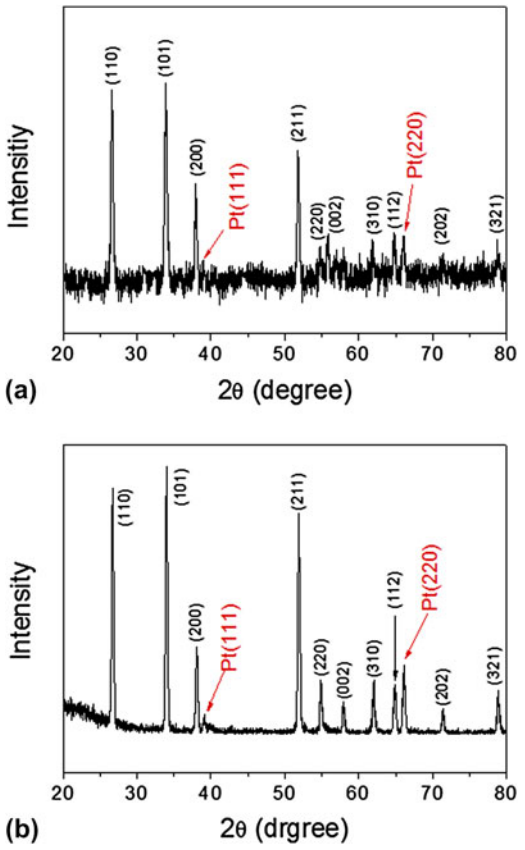


FIG. 7. X-ray θ-2θ diffraction patterns of Pt nanoparticles-decorated SnO_2 nanowires (a) before and (b) after the annealing treatment. Note that the Pt nanoparticles were synthesized by using the same radiolysis condition of Fig. 6.

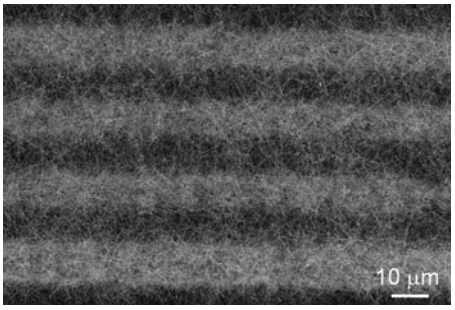


FIG. 8. An FE-SEM image of a fabricated SnO_2 sensor on the PIE-coated substrate.

of the gas concentration. The sensing behaviors can be understood as follows. In air, the SnO_2 nanowire surface will adsorb oxygen species (e.g., O_2^-, O^{2-}, or O^-). By means of the surface reactions, including O_2 (ads) + $e^- \rightarrow O^{2-}$ (ads), O^{2-} (ads) + $e^- \rightarrow 2O^-$(ads), or O^-(ads) + $e^- \rightarrow O^{2-}$ (ads), the conductive electrons in the SnO_2 nanowire are trapped, making the nanowire less conductive. In other words, adsorbed or dissociated oxygen molecules will extract electrons from SnO_2 nanowires. When the SnO_2 nanowire sensor is exposed to the reductive gases, they will

https://doi.org/10.1557/jmr.2012.148 Published online by Cambridge University Press

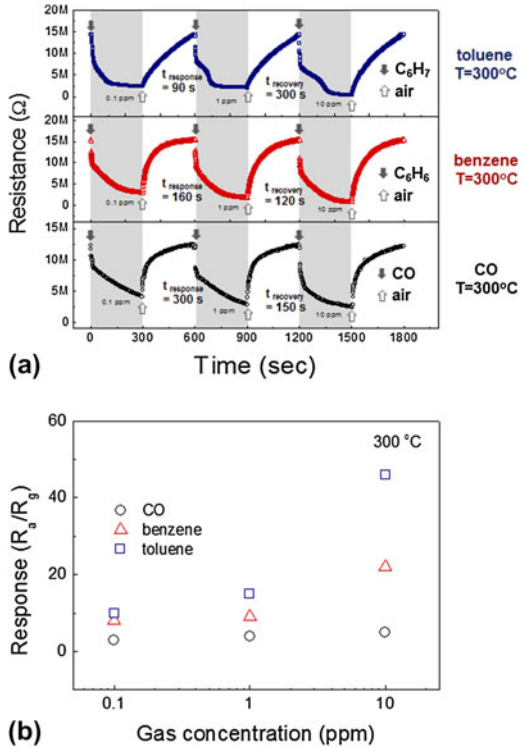


FIG. 9. (a) Response curves and (b) response for the Pt-functionalized SnO_2 nanowires in relation to the concentrations of toluene, benzene and CO.

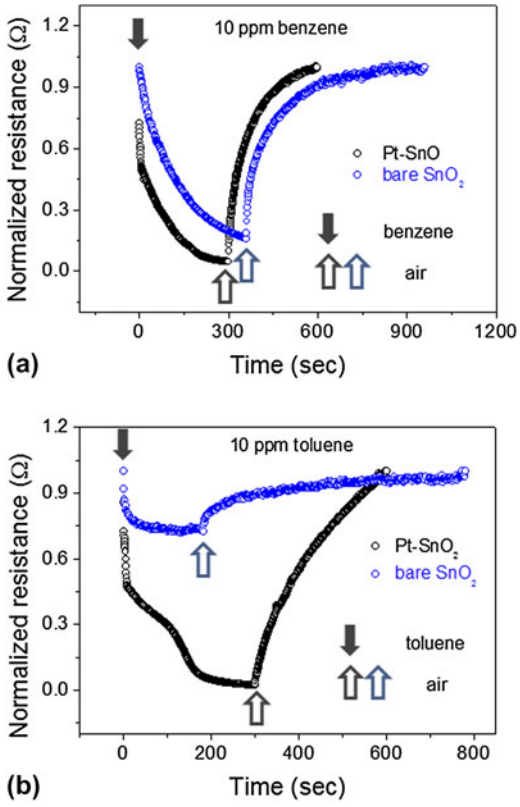


FIG. 10. Sensing performances of the Pt-functionalized SnO_2 nanowires are compared with those of bare SnO_2 nanowires without Pt nanoparticles for (a) 10 ppm benzene and (b) 10 ppm toluene.

react with the oxygen species adsorbed, eventually releasing the electrons back to the conduction band of SnO_2, resulting in an increase of the electrical conductivity. In regard to the Pt functionalization, the response of oxide nanowires to gas molecules is known to be enhanced by the electronic sensitization mechanism[29] and the chemical sensitization mechanism.[30]

In Figs. 10(a) and 10(b), the sensing performances of the Pt-functionalized SnO_2 nanowires are compared with those of bare SnO_2 nanowires without Pt nanoparticles for 10 ppm benzene and toluene, respectively. As shown, bare SnO_2 nanowires show less changes in resistance during supply and stoppage of the target gases, definitely indicating the enhancement of sensing performances by the Pt nanoparticle functionalization. The size and distribution density of Pt nanoparticles may greatly influence the sensing performance. A further study is needed to clarify this.

One of the potential applications of Pt nanoparticles-functionalized SnO_2 nanowires is related to either gas sensors or catalysis. For these applications, the γ-ray radiolysis can be an efficient way of functionalizing oxide nanowires with Pt nanoparticles. According to the results in this work, a precise control of the concentration of solutions and the condition of γ-ray illumination is required to attain aimed size and population density of Pt nanoparticles, which makes the most of Pt-functionalized nanowires in surface-related applications.

IV. CONCLUSION

Pt nanoparticles were synthesized by the γ-ray radiolysis process. The size and formation density of Pt nanoparticles were greatly varied in relation to the processing parameters. A longer exposure time, a lower γ-ray intensity and a higher precursor concentration produced Pt nanoparticles of bigger sizes. Vapor-phase-grown SnO_2 nanowires were uniformly decorated with Pt nanoparticles by the radiolysis process. The sensing performance of the Pt nanoparticle-functionalized SnO_2 nanowires was investigated for CO, toluene and benzene.

ACKNOWLEDGMENT

This work was supported by Nuclear R&D program through the National Research Foundation of Korea.

REFERENCES

1. S. Kundu, S. Panigrahi, S. Praharaj, S. Basu, S.K. Ghosh, A. Pal, and T. Pal: Anisotropic growth of gold clusters to gold nanocubes under UV irradiation. *Nanotechnology* **18**, 075712 (2007).
2. L.B. Scaffardi, N. Pellegri, O. Sanceis, and J.O. Tocho: Sizing gold nanoparticles by optical extinction spectroscopy. *Nanotechnology* **16**, 158 (2005).

https://doi.org/10.1557/jmr.2012.148 Published online by Cambridge University Press

3. J-K. Lung, J-C. Huang, D-C. Tien, C-Y. Liao, K-H. Tseng, T-T. Tsung, W-S. Kao, T-H. Tasi, C-S. Jwo, H-M. Lin, and L. Stobinski: Preparation of gold nanoparticles by arc discharge in water. *J. Alloys Compd.* **434–435**, 655 (2007).
4. A. Henglein and D. Meisel: Radiolytic control of the size of colloidal gold nanoparticles. *Langmuir* **14**, 7392 (1998).
5. Y. Mizukoshi, S. Seino, K. Okitsu, T. Kinoshita, Y. Otome, T. Nakagawa, and T.A. Yamamoto: Sonochemical preparation of composite nanoparticles of Au/γ-Fe_2O_3 and magnetic separation of glutathione. *Ultrason. Sonochem.* **12**, 191 (2001).
6. A. Henglein: Radiolytic preparation of ultrafine colloidal gold particles in aqueous solution: Optical spectrum, controlled growth, and some chemical reactions. *Langmuir* **15**, 6738 (1999).
7. A. Henglein: Reduction of $Ag(CN)_2^-$ on silver and platinum colloidal nanoparticles. *Langmuir* **17**, 2329 (2001).
8. S. Seino, T. Kusunose, and T. Sekino: Synthesis of gold/magnetic iron oxide composite nanoparticles for biomedical applications with good dispersibility. *J. Appl. Phys.* **99**, 08H101 (2006).
9. B. Chwieroth, B.R. Patton, and Y. Wang: Conduction and gas-surface reaction modeling in metal oxide gas sensors. *J. Electroceram.* **6**, 27 (2001).
10. S.S. Kim, J.Y. Park, S-W. Choi, H.S. Kim, H.G. Na, J.C. Yang, and H.W. Kim: Significant enhancement of the sensing characteristics of In_2O_3 nanowires by functionalization with Pt nanoparticles. *Nanotechnology* **21**, 415502 (2010).
11. N. Yamazoe: Toward innovations of gas sensor technology. *Sens. Actuators B* **108**, 2 (2005).
12. G. Neri, A. Bonavita, G. Micali, G. Rizzo, N. Pinna, and M. Niederberger: In_2O_3 and Pt-In_2O_3 nanopowders for low temperature oxygen sensors. *Sens. Actuators B* **127**, 455 (2007).
13. J-K. Choi, I-S. Hwang, S-J. Kim, J-S. Park, S-S. Park, U. Jeong, Y.C. Kang, and J-H. Lee: Design of selective gas sensors using electrospun Pd-doped SnO_2 hollow nanofibers. *Sens. Actuators, B* **150**, 191 (2010).
14. A. Gamez, D. Richard, P. Gallezot, F. Gloguen, R. Faure, and R. Durand: Oxygen reduction on well-defined platinum nanoparticles inside recast ionomer. *Electrochim. Acta* **41**, 307 (1996).
15. O. Antoine, Y. Bultel, and R. Durand: Oxygen reduction reaction kinetics and mechanism on platinum nanoparticles inside nafion. *J. Electroanal. Chem.* **499**, 85 (2001).
16. S. Hrapovic, Y.L. Liu, K.B. Male, and J.H.T. Luong: Electrochemical biosensing platforms using platinum nanoparticles and carbon nanotubes. *Anal. Chem.* **76**, 1083 (2004).
17. Y. Ikariyama, S. Yamaguchi, T. Yukiashi, and H. Ushioda: One-step fabrication of microbiosensor prepared by the codeposition of enzyme and platinum particles. *Anal. Lett.* **20**, 1791 (1987).
18. W. Zhou, L. Xu, M. Wu, L. Xu, and E. Wang: Determination of hydrazines by capillary zone electrophoresis with amperometric detection at a platinum particles-modified carbon fibre microelectrode. *Anal. Chim. Acta* **299**, 189 (1994).
19. G.S. Attand, P.N. Barlett, N.R.B. Coleman, J.M. Elliot, J.R. Owen, and J.H. Wang: Mesoporous platinum films from lyotropic liquid crystalline phases. *Science* **278**, 838 (1997).
20. P.R. Birkin, J.M. Elliot, and Y.E. Watson: Electrochemical reduction of oxygen on mesoporous platinum microelectrodes. *Chem. Commun.* **17**, 1693 (2000).
21. C. Yogi, K. Kojima, T. Takai, and N. Wada: Photocatalytic degradation of methylene blue by Au-deposited TiO_2 film under UV irradiation. *J. Mater. Sci.* **44**, 821 (2009).
22. S-W. Choi, S-H. Jung, and S.S. Kim: Functionalization of selectively grown networked SnO_2 nanowires with Pd nanodots by γ-ray radiolysis. *Nanotechnology* **22**, 225501 (2011).
23. J.Y. Park, S-W. Choi, and S.S. Kim: Junction-tuned SnO_2 nanowires and their sensing properties. *J. Phys. Chem. C* **115**, 12774 (2011).
24. G. Ershov and A. Henglein: Optical spectrum and some chemical properties of colloidal thallium in aqueous solution. *J. Phys. Chem.* **97**, 3434 (1993).
25. J. Belloni: Nucleation, growth and properties of nanoclusters studied by radiation chemistry application to catalysis. *Catal. Today* **113**, 141 (2010).
26. V. Hornebecq, M. Antonietti, T. Cardinal, and M. Treguer-Delapierre: Stable silver nanoparticles immobilized in mesoporous silica. *Chem. Mater.* **15**, 1993 (2003).
27. A. Mayer and M. Antonietti: Investigation of polymer-protected noble metal nanoparticles by transmission electron microscopy: Control of particles morphology and shape. *Colloid Polym. Sci.* **276**, 769 (1998).
28. H.P. Klug and L.E. Alexander: *X-ray Diffraction Procedures for Polycrystalline and Amorphous Materials*, 2nd ed. (Wiley, New York, 1974).
29. M.E. Franke, T.J. Koplin, and U. Simon: Metal and metal oxide nanoparticles in chemiresistors: Dose the nanoscale matter? *Small* **2**, 36 (2006).
30. A. Kolmakov, D.O. Klenov, Y. Lilach, S. Stemmer, and M. Moskovits: Enhanced gas sensing by individual SnO_2 nanowires and nanobelts functionalized with Pd catalyst particles. *Nano Lett.* **5**, 667 (2005).

https://doi.org/10.1557/jmr.2012.148 Published online by Cambridge University Press